CrystEngComm

PAPER

View Article Online
View Journal | View Issue



Cite this: *CrystEngComm*, 2014, **16**, 9651

# The pure-phase $Ba_{3-x}Ca_xSi_6O_{12}N_2$:$Eu^{2+}$ green phosphor: synthesis, photoluminescence and thermal properties

Chuang Wang,[ab] Zhengyan Zhao,[ab] Quansheng Wu,[ab] Shuangyu Xin[ab] and Yuhua Wang*[ab]

Received 5th July 2014,
Accepted 20th August 2014

DOI: 10.1039/c4ce01364f

www.rsc.org/crystengcomm

The promising green oxynitride phosphor, $Ba_{3-x}Ca_xSi_6O_{12}N_2$:$Eu^{2+}$, was synthesized at 1350 °C for 5 hours under a reducing $N_2/H_2$ (5%) atmosphere *via* the solid-state reaction method. The XRD patterns confirm the formation of the pure phase of $Ba_{3-x}Ca_xSi_6O_{12}N_2$:$Eu^{2+}$. With an increase in *x*, the emission spectra shift from 525 nm to 536 nm under near-UV (n-UV) excitation. Accordingly, we propose the underlying mechanisms for the red-shift of the emission spectra by adjusting the cation composition in the host. The influence of the size mismatch on the thermal quenching is also observed. The as-prepared green phosphor exhibits great thermal quenching property, with the remaining 83% of the initial emission intensity measured at 150 °C. The quantum efficiency is measured to be 35.2%. All the results indicate that the $Ba_{3-x}Ca_xSi_6O_{12}N_2$:$Eu^{2+}$ can be a good candidate phosphor applicable to n-UV light-emitting diodes for solid-state lighting.

## 1. Introduction

White light-emitting diodes (LEDs) are considered as the next-generation solid-state lighting sources due to their high efficiency, long lifetime, robustness and environmental friendliness.[1] White LEDs, commercialized in 1996, are commonly fabricated by combining a blue GaInN LED with a yellow $(Y,Gd)_3(Al,Ga)_5O_{12}$:$Ce^{3+}$ (YAG:Ce) phosphor.[2] The YAG:Ce phosphor shows high luminescence efficiency and chemical stability. However, there is a lack of enough red components in its spectrum, making the white LEDs have only a medium color rendering index (CRI) (Ra < 80).[3,4] Until now, the alternative way to solve this problem is the use of UV LEDs with RGB (red, green, blue) phosphors or blue chips with RG phosphors to achieve high CRI values for white LEDs. To attain high color rendition white LEDs (Ra > 80), highly efficient green and red phosphors are generally required. Recently, rare-earth activated nitride/oxynitride luminescent materials have attracted much attention because of their excellent photoluminescence properties for white LED applications, which include $Eu^{2+}$-doped $M_2Si_5N_8$ (M = Ba, Sr and Ca)[5–7] and $CaAlSiN_3$ (ref. 8) red phosphors, β-SiAlON,[9–11] $MSi_2O_2N_2$ (M = Ba, Sr and Ca)[12–15] and $Sr_5Al_{5+x}Si_{21-x}N_{35-x}O_{2+x}$ ($x \approx 0$)[16] green phosphors, and α-SiAlONs,[17,18] as well as $Ce^{3+}$-activated $CaAlSiN_3$,[19] $Y_3Si_6N_{11}$,[20] $La_3Si_6N_{11}$ (ref. 21 and 22) and $SrAlSi_4N_7$ (ref. 23 and 24) yellow phosphors. β-SiAlON:$Eu^{2+}$ is a very promising green phosphor with a narrow emission band (FWHM = 55 nm), which enables it to be widely used in wide color gamut white LED backlights and high color rendition general lighting. However, the synthesis of β-SiAlON:$Eu^{2+}$ usually requires high temperature (1800–2000 °C) and high gas pressure (>1.0 MPa). Therefore, in order to decrease the production cost, it is meaningful to find green-emitting oxynitride phosphors which can be synthesized under ambient conditions. A number of highly efficient green phosphors, including orthosilicate ($Sr_2SiO_4$:$Eu^{2+}$, $Ba_2SiO_4$:$Eu^{2+}$)[25,26] and thiogallate ($MGa_2S_4$:$Eu^{2+}$, M = Ca, Sr, Ba)[27,28] have been developed for application in white LEDs. On the other hand, these phosphors suffer from large thermal quenching and serious moisture sensitivity, making them hard to use in highly reliable white LEDs.

Recently, $Eu^{2+}$ doped green phosphors, $Ba_3Si_6O_{12}N_2$:$Eu^{2+}$, have attracted great attention due to their easy synthesis, high thermal quenching temperature, and high quantum efficiency. Furthermore, they exhibit high color purity and have comparable photoluminescence properties to β-SiAlON:$Eu^{2+}$. Thus they are potentially used for wide color gamut white LEDs.[29–32] Up to now, the research on $Ba_3Si_6O_{12}N_2$:$Eu^{2+}$ has focused on the effect of the $Eu^{2+}$ concentration with various fluxing agents. The most commonly used synthetic methods require high temperature, pressure and some precursors.[30,33,34] These approaches involve either complicated facilities or multi-step processing. To the best of our knowledge, there is

[a] *Department of Materials Science, School of Physical Science and Technology, Lanzhou University, Lanzhou, 730000, China. E-mail: wyh@lzu.edu.cn*
[b] *Key Laboratory for Magnetism and Magnetic Materials of the Ministry of Education, School of Physical Science and Technology, Lanzhou University, Lanzhou 730000, China*

no research on the effects of $Ca^{2+}$ substitution on the structural and luminescence properties of the $Eu^{2+}$ ion by using the solid-state reaction method. In the present study, a series of $Ca^{2+}$-substituted compositions $Ba_{2.9-x}Ca_xSi_6O_{12}N_2:Eu^{2+}$ have been synthesized by the solid-state reaction method. The structural and photoluminescence properties of $Ba_{2.9-x}Ca_xSi_6O_{12}N_2:Eu^{2+}(0 \le x \le 0.36)$ are investigated in detail. Moreover, we propose a hypothesis to explain the mechanism of the emission shift. The influence of the size mismatch on thermal quenching is also discussed.

## 2. Experimental section

### 2.1 Materials and Synthesis

A series of oxynitride phosphors, $Ba_{2.9-x}Ca_xSi_6O_{12}N_2:Eu^{2+}$ were prepared by the solid-state reaction method. The constituent raw materials were $BaCO_3$ (analytical reagents (A.R.)), $CaCO_3$ (A.R.), $Si_3N_4$ (A.R.), $SiO_2$ (A.R.) and $Eu_2O_3$ (99.99%). The raw materials were weighed in appropriate proportions, finely ground, and then sintered in boron nitride (BN) crucibles at 1350 °C for 5 h under a flowing gas of $N_2/H_2$ in a tube furnace. The sintered products were ground again, yielding crystalline powder.

### 2.2 Characterization

All measurements were carried out using the finely ground powder. The phase purity of samples was analyzed by X-ray diffraction (XRD) using a Rigaku D/Max-2400 X-ray diffractometer with Ni-filtered Cu Kα radiation. Photoluminescence (PL) spectra were measured at room temperature using a FLS-920T fluorescence spectrophotometer equipped with a 450 W Xe light source and double excitation monochromators. The PL decay curves were measured using an FLS-920T fluorescence spectrophotometer with an F900nanosecond flash hydrogen lamp as the light source. High-temperature luminescence intensity measurements were carried out by using an aluminum plaque with cartridge heaters; the temperature was measured by thermocouples inside the plaque and controlled by a standard TAP-02 high-temperature fluorescence controller.

## 3. Results and discussion

The phase identification of $Ba_{3-x}Eu_xSi_6O_{12}N_2$ ($x$ = 0.1, 0.15, 0.2, 0.25, 0.3) phosphors characterized by XRD is shown in Fig. 1. Generally, the synthesis of $Ba_3Si_6O_{12}N_2:Eu^{2+}$ often encounters problems of phase purity with orthosilicates formed as impurity phases, which significantly decrease the thermal stability of the green phosphor. The monoclinic $Ba_5Si_8O_{21}$ and orthorhombic $BaSi_2O_5$ are easily formed with larger Si/Ba and O/Ba ratios in the starting powders. Similar to $Ba_3Si_6O_{12}N_2$ consisting of corner-sharing [$SiO_3N$] tetrahedra, both barium orthosilicates were structurally formed by corner-sharing [$SiO_4$] tetrahedra.[35] As can be seen, the high intensity peaks of the as-prepared $Ba_{2.7}Eu_{0.3}Si_6O_{12}N_2$ patterns match well with the reported data of Mikami *et al.*[29] and there is no

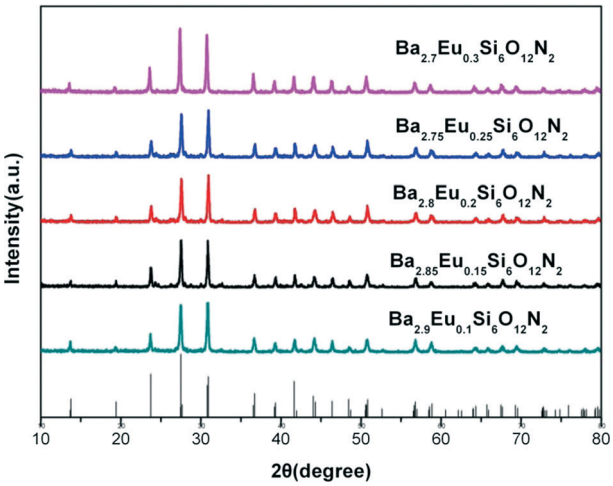


Fig. 1 X-ray diffraction patterns of $Ba_{3-x}Eu_xSi_6O_{12}N_2$ ($x$ = 0.1, 0.15, 0.2, 0.25, 0.3).

detectable impurity phase. The essential factor to obtain the pure phase of $Ba_{3-x}Eu_xSi_6O_{12}N_2$ is by enhancing the $Si_3N_4$ content to suppress the formation of orthosilicates.[35]

Fig. 2 shows the experimental, calculated, and difference results of Rietveld refinement on the XRD patterns of $Ba_{2.7}Eu_{0.3}Si_6O_{12}N_2$ at room temperature. The crystal structure of $Ba_{2.7}Eu_{0.3}Si_6O_{12}N_2$ was analyzed by the Materials Studio program on the basis of the XRD data. The pattern factor $R_p$ and the weighted pattern factor $R_{wp}$ are 8.56% and 11.56%, respectively. The Rietveld refinement on the XRD patterns of $Ba_{2.7}Eu_{0.3}Si_6O_{12}N_2$ obtained herein indicates that the crystallinity is high.

Fig. 3 shows the simulation of the crystal structure of $Ba_3Si_6O_{12}N_2:Eu^{2+}$ by Rietveld refinement. The crystal structure contains a network built up of [$SiO_3N$] tetrahedra. The $Ba^{2+}$ ions occupy two different crystallographic sites; one is

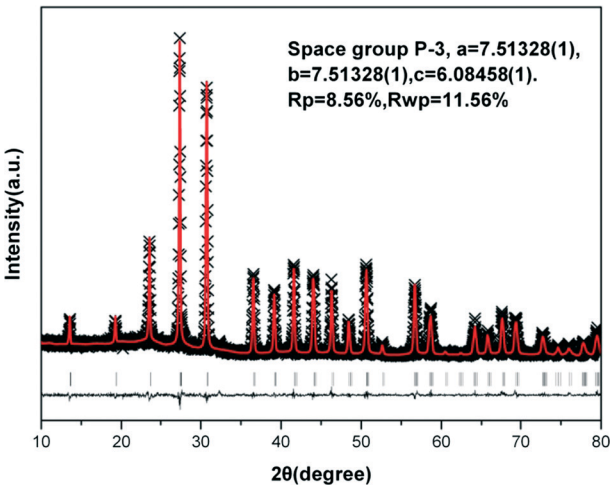


Fig. 2 Rietveld refinement results of the XRD patterns of the $Ba_{2.7}Eu_{0.3}Si_6O_{12}N_2$, including the experimental and calculated intensities as well as differences in intensity between experimental and calculated data.

 

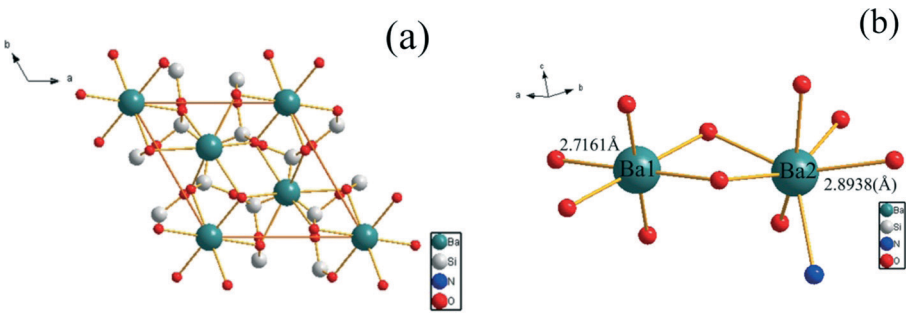


Fig. 3 The simulation of the crystal structure of $Ba_3Si_6O_{12}N_2$:$Eu^{2+}$ by using Rietveld refinement. (a) The view of the $Ba_3Si_6O_{12}N_2$:$Eu^{2+}$ perpendicular to the [001] direction. (b) Coordination spheres of the two different $Ba^{2+}$ sites in $Ba_3Si_6O_{12}N_2$:$Eu^{2+}$.

trigonal anti-prism (distorted octahedron) with six oxygen atoms, and the other is trigonal anti-prism with six oxygen atoms further capped with a nitrogen atom. The excitation and emission spectra of $Ba_{3-x}Eu_xSi_6O_{12}N_2$ ($x$ = 0.1, 0.15, 0.2, 0.25, 0.3) phosphors have been investigated. Fig. 4(a) shows the excitation and emission spectra of the phosphor

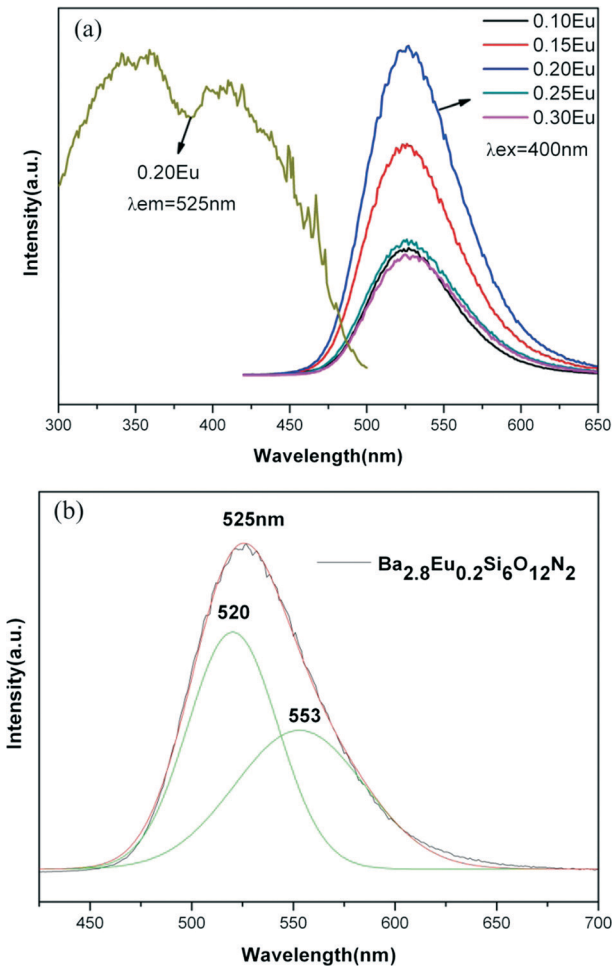


Fig. 4 (a) Excitation and emission spectra ($x$ = 0.1, 0.15, 0.2, 0.25, 0.3) of the as-prepared $Ba_{3-x}Eu_xSi_6O_{12}N_2$. (b) Black lines are the experimental results, and the red line represents the fitting results composed of green lines, which are two Gaussian peaks.

$Ba_{3-x}Eu_xSi_6O_{12}N_2$ ($x$ = 0.1, 0.15, 0.2, 0.25, 0.3). The excitation spectrum of $Ba_{2.8}Eu_{0.2}Si_6O_{12}N_2$ shows a broad band covering the spectral range of 300–450 nm when monitored at $\lambda_{em}$ = 525 nm. The excitation peaks at ~350 nm and ~405 nm are attributable to the $4f^6 5d^1$ multiplets of the $Eu^{2+}$ excited states.[36] The emission spectra of $Ba_{3-x}Eu_xSi_6O_{12}N_2$ ($x$ = 0.1, 0.15, 0.2, 0.25, 0.3) reveal a single broad band centered at 525 nm under 400 nm excitation. Considering the two cation sites of $Ba^{2+}$ in $Ba_{2.8}Eu_{0.2}Si_6O_{12}N_2$, the broad emission band could be fitted to two subbands centered at 520 nm and 553 nm by using Gaussian functions. The Ba1 position has a tight site (6-coordination, Ba1–(N/O) = 2.7161 Å), experiencing stronger crystal field strength, accommodating $Eu^{2+}$ activators to correspond with a lower-energy (longer-wavelength) emission peak (553 nm). However, The Ba2 position has a loose site (7-coordination, Ba2–(N/O) = 2.8938 Å) accommodating $Eu^{2+}$ activators to correspond with a higher-energy (shorter wavelength) emission peak (520 nm).

The influence of the $Eu^{2+}$ concentration on the luminescence properties was also investigated. Fig. 4(a) shows the emission spectra of $Ba_{3-x}Eu_xSi_6O_{12}N_2$ with different $Eu^{2+}$ concentrations. With increasing $Eu^{2+}$ concentration, the luminescence intensity increases and reaches a maximum at $x$ = 0.20. When the $Eu^{2+}$ concentration exceeds 0.20, the concentration quenching occurs.[37] It is mainly attributed to the energy transfer among $Eu^{2+}$ ions. The probability of energy transfer is largely dependent on the distance between the activator ions. With increasing amount of doped $Eu^{2+}$, the distance between $Eu^{2+}$ ions shortens, which increases the probability of non-radiative energy transfer between $Eu^{2+}$ ions. As there is a small overlap between the excitation and emission spectra, the contribution of reabsorption to concentration quenching can be omitted. The critical distance for energy transfer can be roughly calculated using eqn (1),[38]

$$R_c = 2\left(\frac{3V}{4\pi x_c Z}\right)^{1/3} \quad (1)$$

where $x_c$ is the critical concentration of the activator ion, $V$ is the volume of the unit cell, and $Z$ is the number of cations in the unit cell that can be occupied by activator ions. For $Ba_3Si_6O_{12}N_2$:$Eu^{2+}$, $Z$ = 3. Taking $x_c$ = 0.25, $V$ = 315.58 Å$^3$

in eqn (1), the critical distance is then calculated to be about 13.28 Å.

Fig. 5 shows the XRD patterns of the synthesized $Ba_{2.9-x}Ca_xEu_{0.1}Si_6O_{12}N_2$ phosphors at various concentrations ($0.03 \le x \le 0.45$) of $Ca^{2+}$, matching well with the reported data of Mikami *et al.*[29] and no peaks of the raw materials or other allotropic forms are detected when $0.1 \le x \le 0.36$. For doping $Ca^{2+}$ in $Ba_{2.9}Eu_{0.1}Si_6O_{12}N_2$, a small shift in the diffraction peaks is observed (inset in the figure), indicating that the solid solutions are formed.[39] The shift in the diffraction position is due to the changes in the lattice parameters as a result of the difference between the ionic radii of $Ca^{2+}$ (0.100 nm, coordination number = 6) and $Ba^{2+}$ (0.135 nm, coordination number = 6).[40]

Fig. 6 shows the emission spectra of $Ba_{2.9-x}Ca_xEu_{0.1}Si_6O_{12}N_2$ ($x$ = 0.1, 0.15, 0.21, 0.3, 0.36). It is obvious that all the spectral features of the as-synthesized samples are similar. The emission spectra show a single band around 525–536 nm, which are due to the allowed transitions of $Eu^{2+}$ between the excited

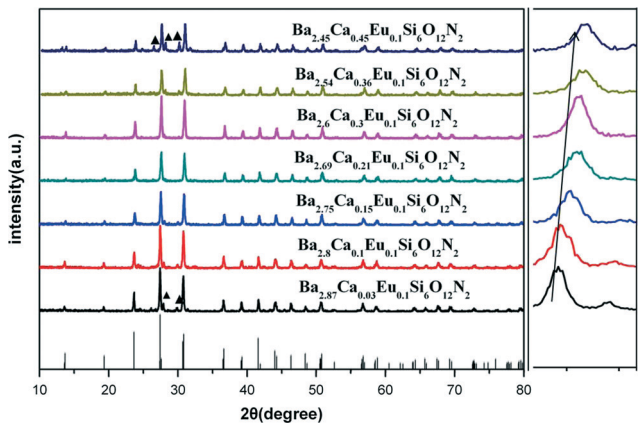


**Fig. 5** X-ray diffraction patterns of $Ba_{2.9-x}Ca_xEu_{0.1}Si_6O_{12}N_2$ ($x$ = 0.03, 0.1, 0.15, 0.21, 0.3, 0.36, 0.45).

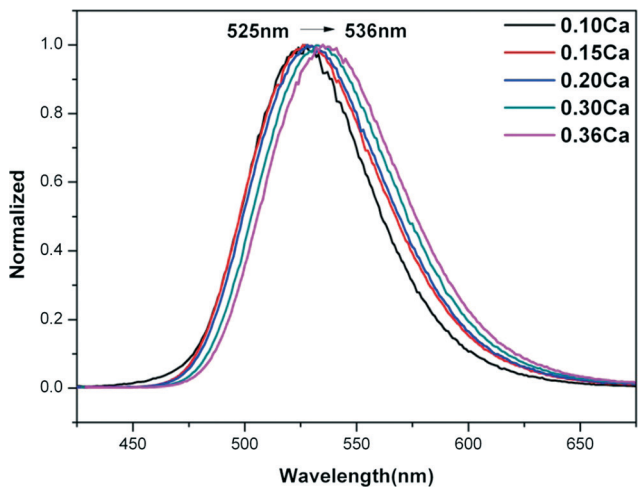


**Fig. 6** Emission spectra of $Ba_{2.9-x}Ca_xEu_{0.1}Si_6O_{12}N_2$ ($x$ = 0.1, 0.15, 0.21, 0.3, 0.36).

5d and the ground 4f levels.[15] The emission peaks shift toward the longer wavelength region from 525 nm ($x$ = 0.1) to 536 nm ($x$ = 0.36) when the $Ca^{2+}$ content increases in the $Ba_{2.9-x}Ca_xEu_{0.1}Si_6O_{12}N_2$ series. It is obvious that with increasing $Ca^{2+}$ content, the corresponding colour tone of the phosphors gradually shifts from green to green-yellow. The red-shift behavior of the emission band can be well explained in terms of an increase in the crystal field which is caused by the increasing $Ca^{2+}$ content in $Ba_{2.9-x}Ca_xEu_{0.1}Si_6O_{12}N_2$.[41] The quantum efficiencies (QE) of $Ba_{2.9-x}Ca_xEu_{0.1}Si_6O_{12}N_2$ for $x$ = 0 and $x$ = 0.3 excited at 400 nm are determined to be 35.2% and 27.2%, respectively. The drastic drop in luminescence efficiency could be due to the mismatch of ionic radii between $Ba^{2+}$ and $Ca^{2+}$, resulting in lattice distortion with higher $Ca^{2+}$ content in the lattice.[42] The lower QE could be further enhanced by process optimization.

The thermal quenching properties are important in the LED application. The thermal quenching properties of $Ba_{2.9-x}Ca_xEu_{0.1}Si_6O_{12}N_2$ samples were investigated. Fig. 7(a) and (b) present the temperature-dependent photoluminescence spectra of $Ba_{2.9-x}Ca_xEu_{0.1}Si_6O_{12}N_2$ with 400 nm excitation for $x$ = 0 and 0.3, respectively. An obvious blue-shift was observed in the spectra when the temperature increased from 20 °C to 230 °C for both samples. This phenomenon can be ascribed to the thermally active phonon-assisted tunneling from the excited states of the lower-energy emission band to those of the higher-energy emission band in the configuration coordinate diagram.[43–45] Fig. 7(c) displays the temperature dependence of the PL intensity of $Ba_{2.9-x}Ca_xEu_{0.1}Si_6O_{12}N_2$ ($x$ = 0, 0.3). By increasing the temperature to 150 °C (the working temperature for white LEDs), the emission intensity of the $Ba_{2.9-x}Ca_xEu_{0.1}Si_6O_{12}N_2$ ($x$ = 0, 0.3) phosphor remains at 83% and 74% of that measured at room temperature, and the emission intensity of $Ba_{2.6}Ca_{0.3}Eu_{0.1}Si_6O_{12}N_2$ decreases faster with increasing temperature compared to that of $Ba_{2.9}Eu_{0.1}Si_6O_{12}N_2$, which indicates that the doping of $Ca^{2+}$ is a disadvantage to the thermal stability. It can be explained by the configurational coordinate diagram in Fig. 7(d). The curve g is the ground state of $Eu^{2+}$. The curves e1 and e2 are the excited states of $Eu^{2+}$ of the $[EuO_6]^{10-}$ octahedron neighboring with the $[BaO_6]^{10-}$ and $[CaO_6]^{10-}$ octahedra, respectively. $\Delta R$ is the departure from the ground state to the excited states along the $R$ axis. A and B are the crossing points of g and e1 and e2, respectively. C and D are the lowest positions of the e1 and e2 curves, respectively. $\Delta E1$ and $\Delta E2$ are the energy differences of D to A and C to B, respectively. In our experiment, the concentration of $Eu^{2+}$ is low, and thus the distance between two $Eu^{2+}$ ions is larger. To simplify the question, we assume that the $Eu^{2+}$ is non-interacting. Under UV light, the electrons are excited to the excited states from g to e1 and e2. At room temperature, most of the electrons return to the ground state *via* ways ① and ②, but with the increase in temperature, more electrons return to the ground state *via* ways ③ and ④ from the crossing points A and B due to the electron–phonon coupling. In our experiment, the doping of the $Ca^{2+}$ greatly changes the crystal field and the nephelauxetic effect, and then affects the position of the

 

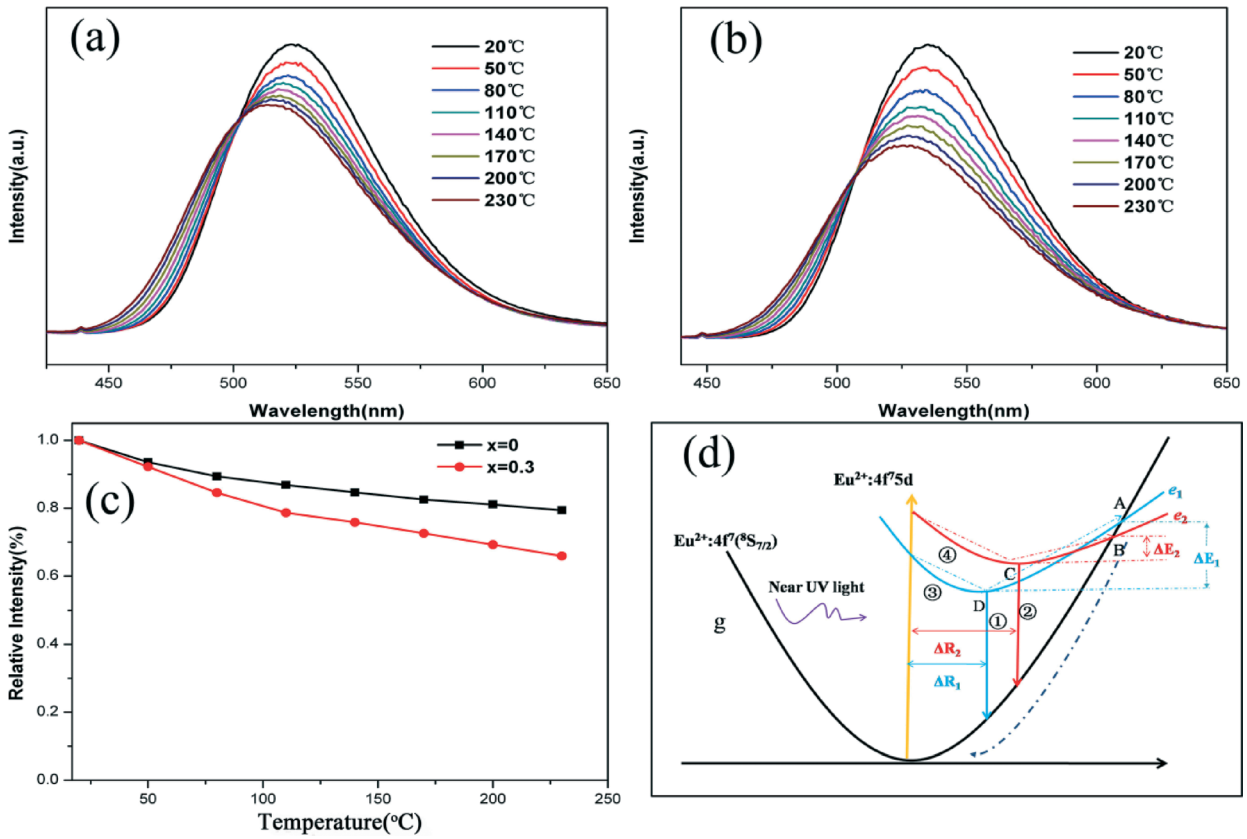


**Fig. 7** The PL spectra of (a) $Ba_{2.9}Eu_{0.1}Si_6O_{12}N_2$ and (b) $Ba_{2.6}Ca_{0.3}Eu_{0.1}Si_6O_{12}N_2$ phosphors under various temperatures. (c) The dependence of normalized PL intensities on temperature for phosphors, excited at 400 nm. (d) The configurational coordinate diagram of the ground state of $Eu^{2+}$ and the excited states of $Eu^{2+}$ located in the two different crystal environments.

crossing points A and B of the ground state and excited states; furthermore, the doping determines the value of $\Delta E$. According to the results of the thermal properties herein, the mechanism of the thermal quenching is illustrated in Fig. 7(d); the crossing point B is located below the crossing point A, that is, $\Delta E1 > \Delta E2$. Therefore, the doping of $Ca^{2+}$ is not beneficial to the thermal properties.

## 4. Conclusion

In summary, a simple solid-state route was adopted to prepare a series of oxynitride phosphors, $Ba_{2.9-x}Ca_xEu_{0.1}Si_6O_{12}N_2$ ($x$ = 0.1, 0.15, 0.21, 0.3, 0.36), which could be used to tune the photoluminescence properties and thermal stability in the related size-mismatched cation-substituted phosphors. The PLE spectra span the UV to the blue region, and the PL spectra show green-yellow emission under 400 nm excitation. With various crystal environments in the $Ba_{2.9-x}Ca_xEu_{0.1}Si_6O_{12}N_2$ structure, the emission spectra can be tuned from 525 nm to 536 nm, and the mechanism of emission shift was identified. The decrease in thermal stability with the $Ca^{2+}$ incorporation can be explained from the configurational coordinate diagram. All these results indicate that the $Ba_{2.9-x}Ca_xEu_{0.1}Si_6O_{12}N_2$ phosphor is a potential candidate for n-UV LED applications.

## Acknowledgements

This work is supported by the National Science Foundation for Distinguished Young Scholars (no. 50925206) and Specialized Research Fund for the Doctoral Program of Higher Education (no. 20120211130003).

## Notes and references

1 R.-J. Xie, Y. Q. Li, N. Hirosaki and H. Yamamoto, *Nitride Phosphors and Solid-State lighting*, Taylor & Francis, Boca Raton, 2011, pp. 2–69.
2 R.-J. Xie, N. Hirosaki, K. Sakuma, Y. Yamamoto and M. Mitomo, *Appl. Phys. Lett.*, 2004, **84**, 5404.
3 M. Yamada, T. Naitou, K. Izuno, H. Tamaki, Y. Murazaki, M. Kameshima and T. Mukai, *Jpn. J. Appl. Phys.*, 2003, **42**, L20–L23.
4 H. S. Jang, W. B. Im, D. C. Lee, D. Y. Jeon and S. S. Kim, *J. Lumin.*, 2007, **126**, 371–377.
5 Y. Q. Li, J. E. J. van Steen, J. W. H. van Krevel, G. Botty, A. C. A. Delsing, F. J. DiSalvo, G. de With and H. T. Hintzen, *J. Alloys Compd.*, 2006, **417**, 273–279.
6 R. J. Xie, N. Hirosaki, T. Suehiro, F.-F. Xu and M. Mitomo, *Chem. Mater.*, 2006, **18**, 5578–5583.

7 J.-M. Song, J.-S. Park and S. Nahm, *Ceram. Int.*, 2013, **39**, 2845–2850.
8 K. Uheda, N. Hirosaki, Y. Yamamoto, A. Naito, T. Nakajima and H. Yamamoto, *Electrochem. Solid-State Lett.*, 2006, **9**, H22–H25.
9 N. Hirosaki, R. J. Xie, K. Kimoto, T. Sekiguchi, Y. Yamamoto, T. Suehiro and M. Mitomo, *Appl. Phys. Lett.*, 2005, **86**, 211905.
10 R. J. Xie, N. Hirosaki, H. L. Li, Y. Q. Li and M. Mitomo, *J. Electrochem. Soc.*, 2007, **154**, J314.
11 K. Kimoto, R. J. Xie, Y. Matsui, K. Ishizuka and N. Hirosaki, *Appl. Phys. Lett.*, 2009, **94**, 041908.
12 J. Botterman, K. V. D. Eeckhout, A. J. J. Bos, P. Dorenbos and P. F. Smet, *Opt. Mater. Express*, 2012, **2**, 341–349.
13 V. Bachmann, T. Jüstel, A. Meijerink, C. Ronda and P. J. Schmidt, *J. Lumin.*, 2006, **121**, 441–449.
14 I. H. Cho, G. Anoop, D. W. Suh, S. J. Lee and J. S. Yoo, *Opt. Mater. Express*, 2012, **2**, 1292–1305.
15 V. Bachmann, C. Ronda, O. Oeckler, W. Schnick and A. Meijerink, *Chem. Mater.*, 2009, **21**, 316–325.
16 O. Oeckler, J. A. Kechele, H. Koss, P. J. Schmidt and W. Schnick, *Chem. – Eur. J.*, 2009, **15**, 5311–5319.
17 R. J. Xie, N. Hirosaki, M. Mitomo, Y. Yamamoto, T. Suehiro and N. Ohashi, *J. Am. Ceram. Soc.*, 2004, **87**, 1308–1370.
18 R. J. Xie, N. Hirosaki, M. Mitomo, T. Suehiro, X. Xu and H. Tanaka, *J. Am. Ceram. Soc.*, 2005, **88**, 2883–2888.
19 Y. Q. Li, N. Hirosaki, R. J. Xie, T. Takeda and M. Mitomo, *Chem. Mater.*, 2008, **20**, 6704–6714.
20 L. Liu, R. J. Xie, W. Li, N. Hirosaki, Y. Yamamoto, X. Sun and D. Johnson, *J. Am. Ceram. Soc.*, 2013, **96**, 1688–1690.
21 T. Seto, N. Kijima and N. Hirosaki, *ECS Trans.*, 2009, **25**, 247–252.
22 T. Suehiro, N. Hirosaki and R. J. Xie, *ACS Appl. Mater. Interfaces*, 2011, **3**, 811–816.
23 J. Ruan, R. J. Xie, S. Funahashi, Y. Tanaka, T. Takeda, T. Suehiro, N. Hirosaki and Y.-Q. Li, *J. Solid State Chem.*, 2013, **208**, 50–57.
24 L. Zhang, J. Zhang, X. Zhang, Z. Hao, H. Zhao and Y. Luo, *ACS Appl. Mater. Interfaces*, 2013, **5**, 12839–12846.
25 J. H. Lee and Y. J. Kim, *Mater. Sci. Eng., B*, 2008, **146**, 99–102.
26 M. A. Lim, J. K. Park, C. H. Kim, H. D. Park and M. W. Han, *J. Mater. Sci. Lett.*, 2003, **22**, 1351–1353.
27 T. E. Peters and J. A. Baglio, *J. Electrochem. Soc.*, 1972, **119**, 230–236.
28 Y. Pan, M. Wu and Q. Su, *Mater. Sci. Eng., B*, 2004, **106**, 251–256.
29 M. Mikami, S. Shimooka, K. Uheda, H. Imura and N. Kijima, *Key Eng. Mater.*, 2009, **403**, 11–14.
30 C. Braun, M. Seibald, S. L. Borger, O. Oeckler, T. D. Boyko, A. Moewes, G. Miehe, A. Tucks and W. Schnick, *Chem. – Eur. J.*, 2010, **16**, 9646–9657.
31 I. Sun Cho, D. Kyun Yim, C. Hyun Kwak, J. Sul An, H. Suk Roh and K. Sun Hong, *J. Lumin.*, 2012, **132**, 375–380.
32 Y. Q. Li, A. C. A. Delsing, G. de With and H. T. Hintzen, *Chem. Mater.*, 2005, **17**, 3242–3248.
33 Y. H. Song, T. Y. Choi, K. Senthil, T. Masaki and D. H. Yoon, *Mater. Lett.*, 2011, **65**, 3399–3401.
34 E. H. Kang, S. W. Choi and S. H. Hong, *ECS J. Solid State Sci. Technol.*, 2012, **1**, R11–R14.
35 Wanyuan Li, Rong-Jun Xie, Tianliang Zhou, L. Liu and Y. Zhu, *Dalton Trans.*, 2014, **43**, 6132–6138.
36 Y. Q. Li, J. Van Steen, J. Van Krevel, G. Botty, A. Delsing, F. DiSalvo and H. Hintzen, *J. Alloys Compd.*, 2006, **417**, 273–279.
37 Wanyuan Li, Rong-Jun Xi, Tianliang Zhou, L. Liu and Y. Zhu, *Dalton Trans.*, 2014, **43**, 6132–6138.
38 G. Blasse, *Phys. Lett. A*, 1968, **28**, 444–445.
39 C. R. Volker Bachmann, O. Oeckler, W. Schnick and A. Meijerink, *Chem. Mater.*, 2009, **21**, 316–325.
40 R. D. Shannon, *Acta Crystallogr., Sect. A: Cryst. Phys., Diffr., Theor. Gen. Crystallogr.*, 1976, **32**, 751.
41 Y. Q. Li, A. C. A. Delsing, G. de With and H. T. Hintzen, *Chem. Mater.*, 2005, **17**(50), 3242–3248.
42 W.-R. Liu, C.-W. Yeh, C.-H. Huang, C. C. Lin, Y.-C. Chiu, Y.-T. Yeh and R.-S. Liu, *J. Mater. Chem.*, 2011, **21**, 3740.
43 J. S. Kim, Y. H. Park, S. M. Kim, J. C. Choi and H. L. Park, *Solid State Commun.*, 2005, **133**, 445–448.
44 J. Ruan, R.-J. Xie, N. Hirosaki and T. Takeda, *J. Am. Ceram. Soc.*, 2011, **94**, 536–542.
45 Z. Xia, X. Wang, Y. Wang, L. Liao and X. Jing, *Inorg. Chem.*, 2011, **50**, 10134–10142.

 